Applied Physics Letters ARTICLE pubs.aip.org/aip/apl

Device physics of indoor photovoltaics: A fundamental investigation

Cite as: Appl. Phys. Lett. **127**, 193902 (2025); doi: 10.1063/5.0283842
Submitted: 3 June 2025 · Accepted: 23 October 2025 ·
Published Online: 10 November 2025

View Online Export Citation CrossMark

Zhouqing Wei,[1,2] Xin Wen,[1,2] Wenbo Lu,[1,2] Xiaoyan An,[1,2] Qingxiang Liu,[1,2] Yunpei Zhang,[2] Di Wu,[2] Huan Yang,[3] Jin-Song Hu,[1,2] and Ding-Jiang Xue[1,2,a)]

AFFILIATIONS

[1]Beijing National Laboratory for Molecular Sciences (BNLMS), CAS Key Laboratory of Molecular Nanostructure and Nanotechnology, Institute of Chemistry, Chinese Academy of Sciences (CAS), Beijing 100190, China
[2]University of Chinese Academy of Sciences, Beijing 100049, China
[3]School of Chemistry and Materials Science, Shanxi Normal University, Taiyuan 030032, China

Note: This paper is part of the Special Topic, High-Performance Thin-Film Indoor Photovoltaics.
[a)]**Author to whom correspondence should be addressed:** djxue@iccas.ac.cn

ABSTRACT

Indoor photovoltaics (IPVs) have recently attracted considerable attention due to their ability to harvest indoor light to power Internet of Things (IoT) devices. However, in contrast to the well-established device physics of solar cells, research on IPV device physics remains limited, hindering the development of this emerging field. Here, we apply the Shockley–Queisser (SQ) theory to systematically investigate the device physics of IPVs. Through the comparative analysis of spectral differences between standard sunlight and indoor light sources, we calculate the SQ-limited short-circuit current density (J_{sc}), open-circuit voltage (V_{oc}), and fill factor (FF) as functions of the absorber material's bandgap. We reveal that J_{sc} exhibits a linear dependence on illuminance; V_{oc} remains nearly constant across varying illumination levels; and FF necessitates a large shunt resistance to retain high values. Based on these PV parameters, we finally calculated the SQ-limited power conversion efficiency (PCE), demonstrating an optimal bandgap range of 1.8–1.9 eV for IPVs, which achieves a PCE limit of approximately 55%.

Published under an exclusive license by AIP Publishing. https://doi.org/10.1063/5.0283842

16 November 2025 15:40:56

With the rapid development of the Internet of Things (IoT), billions of IoT devices that collect, analyze, and transmit data from the physical world to the internet network have been installed recently.[1,2] Considering that most IoT terminal devices are connected through wireless communication systems, they operate independently of the electrical grid, making off-grid power systems imperative.[3,4] Currently, the prevailing portable power supply for such wireless devices comes from batteries.[4,5] However, batteries exhibit a relatively limited lifespan, and replacing or charging them would be a tremendous task and introduce disruptions to the seamless data transmission.[5] In this regard, indoor photovoltaics (IPVs), which harvest and convert indoor ambient light into usable electrical power, can directly power wireless devices or charge batteries, given that a significant portion of wireless IoT devices is located inside buildings.[6–8]

Several types of PVs have shown remarkable progress in this emerging area. Perovskite PVs have achieved indoor power conversion efficiencies (PCEs) of up to 40% under 1000 lux illumination,[9–11] while organic photovoltaics and dye-sensitized cells have reached indoor PCEs above 30% under the same illumination.[12–15] Furthermore, the world's first solar cells built from selenium have achieved an indoor PCE of 20.1% under 1000 lux illumination.[16–19] These high-performance IPVs now sustainably power various wireless IoT devices.[8,16,17] Moreover, standardized testing protocols for IPV performance have been established, providing a foundation for the sustainable development of IPVs.[20] However, despite these advances, the fundamental device physics of IPVs remains limited, restricting further development in this field.

In this Letter, we report a systematic investigation of the IPV device physics using the Shockley–Queisser (SQ) theory. We calculate the SQ-limited short-circuit current density (J_{sc}), open-circuit voltage (V_{oc}), and fill factor (FF) as functions of the absorber material's bandgap. By integrating these parameters, we finally calculate the SQ-limited indoor PCE, which reveals an optimal bandgap range of 1.8–1.9 eV for IPVs, achieving a theoretical PCE limit of ∼55%.

We began by comparing the solar and indoor light emission spectra. The incident light source for solar cells is typically standardized to

Published under an exclusive license by AIP Publishing

the AM1.5G spectral irradiance, whereas IPV devices predominantly operate under indoor artificial light sources, which are typically designed to align with the photopic luminosity function $V(\lambda)$ of human eyes [Fig. 1(a)], within the 400–700 nm visible range.[21,22] Consequently, optimal artificial light source designs require spectral confinement within this photobiologically active window.

We then measured the emission spectra of commonly used indoor light sources, including three representative light-emitting diodes (LEDs) with correlated color temperatures (CCTs) of 2700, 4000, and 6500 K. As previously reported,[20] spectral irradiance measurements of LEDs were performed in a homemade testing box with all black internal components and equipped with a baffle to eliminate the effects caused by scattered and stray light. By optimizing the number of LEDs and the distance configuration, the spectrometer was positioned within a spatially homogeneous illumination field with a homogeneity factor (H_f) below 1%, thus satisfying IPV measurements. Figure 1(b) confirms that the emissions of all three CCT LEDs are intentionally narrowed to the visible range (400–700 nm). Increasing the CCT induces a hypsochromic spectral shift, enhancing the blue emission (450–480 nm) while attenuating the yellow-green components (550–580 nm) (Fig. S1). Based on the emission spectra of LEDs, we conclude that the fundamental distinction between solar and LED illumination lies in their spectral coverage divergence: solar radiation spans ultraviolet to infrared (300–2500 nm), while LEDs are confined to the visible spectrum (400–700 nm).

According to the measured spectral irradiance $\Phi(\lambda)$ of LEDs, we then calculated the corresponding input light power density (P_{in}) using the following equation:[23]

$$P_{in} = \int_0^\infty \Phi(\lambda) d\lambda, \tag{1}$$

since the PCE of a PV cell is determined by the equation

$$\mathrm{PCE} = \frac{P_{out}}{P_{in}}, \tag{2}$$

where P_{out} is the output power density of the PV cell. Based on the calculated P_{in} of LEDs, we further conclude that another significant difference between solar and LED illumination is the light power density: indoor light at 1000 lux exhibits approximately three orders of magnitude lower density than that under AM1.5G illumination. Notably, when evaluating indoor lighting conditions, the commonly used physical quantity is illuminance (L, measured in lux) rather than P_{in}. The relationship between L and P_{in} is determined by the following equations:[24]

$$L = K_r P_{in} \int_0^\infty \Phi(\lambda)_{norm} V(\lambda) d\lambda, \tag{3}$$

$$\Phi(\lambda)_{norm} = \frac{\Phi(\lambda)}{\int_0^\infty \Phi(\lambda) d\lambda}, \tag{4}$$

where K_r is a constant with a value of 683.002 lm W^{-1}, and $\Phi(\lambda)_{norm}$ is the normalized emission spectrum of the light source.[24] As shown in Eq. (3), L is directly proportional to the light power density P_{in} for the same light source. We measured the spectral irradiance of LEDs with CCTs of 2700, 4000, and 6500 K under illumination levels ranging from 100 to 1000 lux (Fig. S2), and calculated the corresponding P_{in} using Eq. (1). Notably, the integral term in Eq. (3) retains a constant value (Fig. S3), indicating that L is directly proportional to the light power density P_{in} for the same light source. Figure 1(c) plots the P_{in} as a function of L, revealing a distinct linear relationship that aligns closely with Eq. (3). Due to the lower integral term, the 6500 K LED requires a higher P_{in} to achieve the same illuminance.

We next discussed the three key PV parameters including J_{sc}, V_{oc}, and FF, since the PCE of a PV cell can be determined by the following equation:

$$\mathrm{PCE} = \frac{J_{sc} \times V_{oc} \times \mathrm{FF}}{P_{in}}. \tag{5}$$

The above-mentioned three parameters for ideal PV cells can be described using the following Shockley equation:[25]

$$J = J_0 \left[\exp\left(\frac{qV}{nkT}\right) - 1 \right] - J_{ph}, \tag{6}$$

where J_0 is the reverse saturation current, q is the elementary charge, n is the diode ideality factor ($n = 1$ for ideal photovoltaic cell), k is the Boltzmann constant, T is the temperature of the cell (300 K is commonly used), and J_{ph} is the generated photocurrent density. In this regard, J_{sc} represents the current density obtained under short-circuit situation, V_{oc} is the voltage obtained under open-circuit situation, and FF is defined as follows:

$$\mathrm{FF} = \frac{(JV)_{max}}{J_{sc} V_{oc}}, \tag{7}$$

where $(JV)_{max}$ is the point of maximum power output in the $J - V$ curve.

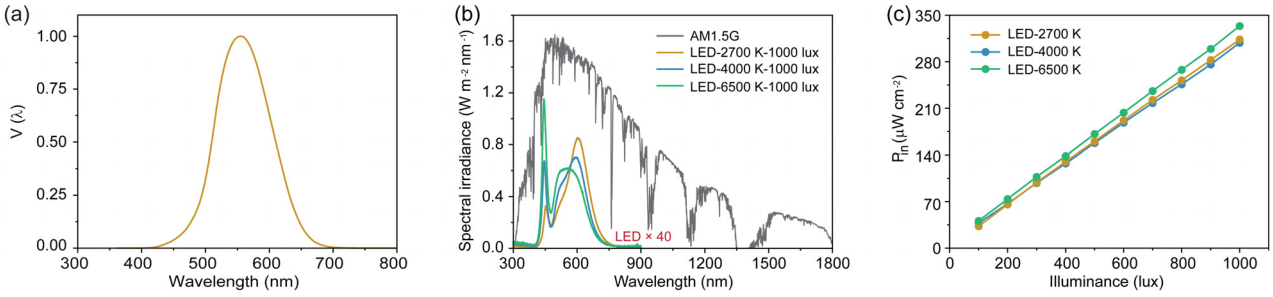

FIG. 1. (a) Photopic spectral luminous efficiency function for human vision. (b) Comparison of the emission spectra of AM1.5G solar, 2700, 4000, and 6500 K LEDs at 1000 lux. Note that the spectral irradiance intensities of the LEDs are amplified by 40 times for clear demonstration. (c) P_{in} of 2700, 4000, and 6500 K LEDs at different illuminance.

16 November 2025 15:40:56

Published under an exclusive license by AIP Publishing

We first discussed J_{sc}. As shown in Eq. (6), J_{sc} is equal to J_{ph}, when the voltage is zero. According to the SQ theory,[26] the J_{ph} is expressed by the following equation:[27]

$$J_{sc} = J_{ph} = q\int_0^{\infty} \mathrm{EQE}_{PV}(E)\Phi(E)dE, \tag{8}$$

where E is the energy of photon, $\Phi(E)$ is the spectral photon flux of the light source, $\mathrm{EQE}_{PV}(E)$ is the energy-dependent external quantum efficiency of the PV cell. Ideally, the $\mathrm{EQE}_{PV}(E)$ can be expressed as follows:[27]

$$\mathrm{EQE}_{PV}^{SQ}(E) = 0, \quad E < E_g; \quad \mathrm{EQE}_{PV}^{SQ}(E) = 1, \quad E \geq E_g. \tag{9}$$

In this case, the PV cell has a theoretical maximum J_{sc}, called J_{sc}^{SQ}, which can be calculated as follows:

$$J_{sc}^{SQ} = q\int_0^{\infty} \mathrm{EQE}_{PV}^{SQ}(E)\Phi(E)dE = q\int_{E_g}^{\infty} \Phi(E)dE. \tag{10}$$

Experimentally, the wavelength-dependent spectral irradiance $\Phi(\lambda)$ is measured using a spectrometer. The $\Phi(E)$ is derived and then calculated through the following equation:[24]

$$\Phi\left(E = \frac{hc}{\lambda}\right) = \Phi(\lambda)\frac{\lambda^3}{h^2c^2}. \tag{11}$$

We then substituted $\Phi_{AM1.5G}(\lambda)$ and $\Phi_{LED}(\lambda)$ into Eqs. (10) and (11), respectively, and calculated the J_{sc}^{SQ} as a function of the absorber material's bandgap under AM1.5G and LED illumination. Figure 2(a) shows the J_{sc}^{SQ} curves under AM1.5G solar illumination (100 mW cm^{-2}) and under LED illumination with CCTs of 2700, 4000, and 6500 K at 1000 lux. We observed that the calculated J_{sc}^{SQ} under LED illumination at 1000 lux is approximately 2–3 orders of magnitude lower than that under AM1.5G solar illumination, primarily due to the lower light power density. Under AM1.5G solar illumination, the calculated J_{sc}^{SQ} monotonically increases as the bandgap of absorber material decreases. The plateaus are due to gaps in the AM1.5G spectrum arising from atmospheric absorption.[28] In contrast to AM1.5G illumination, under LED illumination with emission spectra concentrated in the visible range, a monotonic increase in J_{sc}^{SQ} is observed as the bandgap decreases from 3.1 to 1.6 eV. Further reduction of the bandgap below 1.6 eV leads to current density saturation, as photons within the indoor spectral range (400–700 nm) are already nearly fully absorbed. Furthermore, the J_{sc}^{SQ} curves exhibit identical trends under LED sources with the same CCT, despite variations in illuminance (Fig. S4). Figures 2(b)–2(d) demonstrate that J_{sc}^{SQ} for fixed-bandgap absorber materials under the same light source exhibits a linear dependence on illuminance, while gradual saturation occurs as the bandgap decreases to approximately 1.7 eV.

We subsequently focused on the discussion of V_{oc}. Based on the Shockley equation, V_{oc} can be derived by setting $J = 0$ in Eq. (6) as follows:[27]

$$V_{oc} = \frac{kT}{q}\ln\left(\frac{J_{sc}}{J_0} + 1\right), \tag{12}$$

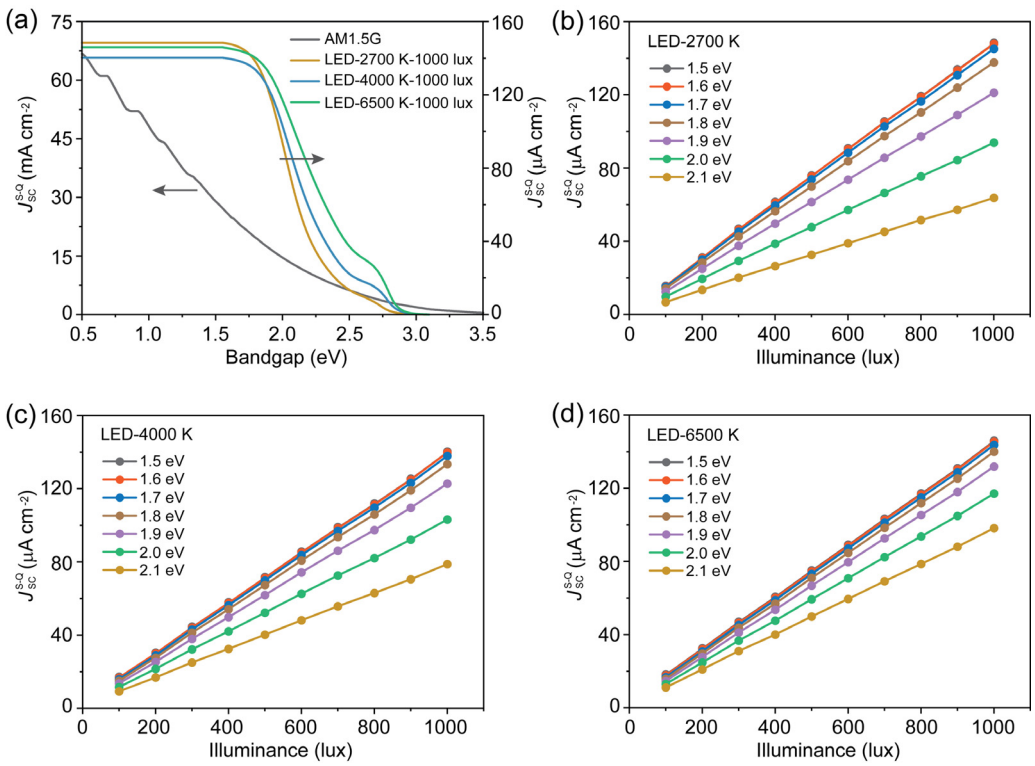

FIG. 2. (a) Bandgap-dependent J_{sc}^{SQ} for AM1.5G solar and 2700, 4000, and 6500 K LEDs at 1000 lux. The variation of J_{sc}^{SQ} vs illuminance of the absorber materials with various bandgaps under (b) 2700 K, (c) 4000 K, and (d) 6500 K LEDs, respectively.

16 November 2025 15:40:56

Published under an exclusive license by AIP Publishing

where J_0 includes contributions from both radiative and non-radiative recombination currents.[29] According to the SQ theory, the minimum value of J_0 (J_0^{SQ}) originates from blackbody radiation, which can be expressed as follows:[27]

$$J_0^{SQ} = q\int_{E_g}^{\infty} \Phi_{BB}(E)dE, \tag{13}$$

where $\Phi_{BB}(E)$ is the spectral photon flux of the black body at $T = 300$ K, given by[29]

$$\Phi_{BB}(E) = \frac{2\pi E^2}{h^3c^2}\frac{1}{\left[\exp\left(\frac{E}{kT}\right)-1\right]}. \tag{14}$$

We then calculated the SQ limit of V_{oc} (V_{oc}^{SQ}) through the following equation:

$$V_{oc}^{SQ} = \frac{kT}{q}\ln\left(\frac{J_{sc}^{SQ}}{J_0^{SQ}}+1\right) = \frac{kT}{q}\ln\left[\frac{q\int_{E_g}^{\infty}\Phi_{light}(E)dE}{q\int_{E_g}^{\infty}\Phi_{BB}(E)dE}+1\right]. \tag{15}$$

Figure 3(a) shows that V_{oc}^{SQ} increases monotonically with the bandgap in the range from 0.5 to 3.5 eV. For LEDs with different CCTs, the V_{oc}^{SQ} remains essentially the same under the same illuminance.

The V_{oc} loss (V_{loss}) is a key metric for evaluating nonideal energy losses in PVs, which can be defined as

$$\begin{aligned} V_{loss} &= \frac{E_g}{q} - V_{oc}^{actual} \\ &= \left(\frac{E_g}{q} - V_{oc}^{SQ}\right) + \left(V_{oc}^{SQ} - V_{oc}^{rad}\right) + \left(V_{oc}^{rad} - V_{oc}^{actual}\right) \\ &= \Delta V_1 + \Delta V_2 + \Delta V_3. \end{aligned} \tag{16}$$

The first component (ΔV_1) arises from the radiative recombination loss above the gap.[21] Thermodynamic analysis indicates that ΔV_1 includes Carnot loss resulting from the conversion of thermal energy into entropy free work, angle entropy loss (or Boltzmann loss) arising from the mismatch between absorption and re-emission solid angles, and voltage recoupment as a result of carrier cooling.[30–32] Figure 3(b) shows that ΔV_1 increases as the bandgap increases from 0.5 to 3.5 eV, rising from about 0.2 V to 0.4 V under AM1.5G illumination and from about 0.35 to 0.55 V under LED illumination.

The second component (ΔV_2) is the offset between V_{oc}^{SQ} and the open-circuit voltage in the radiative limit (V_{oc}^{rad}), where only radiative recombination is allowed.[27] Specifically, in the SQ theory, the band edge of the material is completely abrupt, whereas in practical cases, the band edge is gradual, arising from the $EQE_{PV}(E)$.[27] We then derived the expression for V_{oc}^{rad} by modifying V_{oc}^{SQ} with the addition of $EQE_{PV}(E)$,[27]

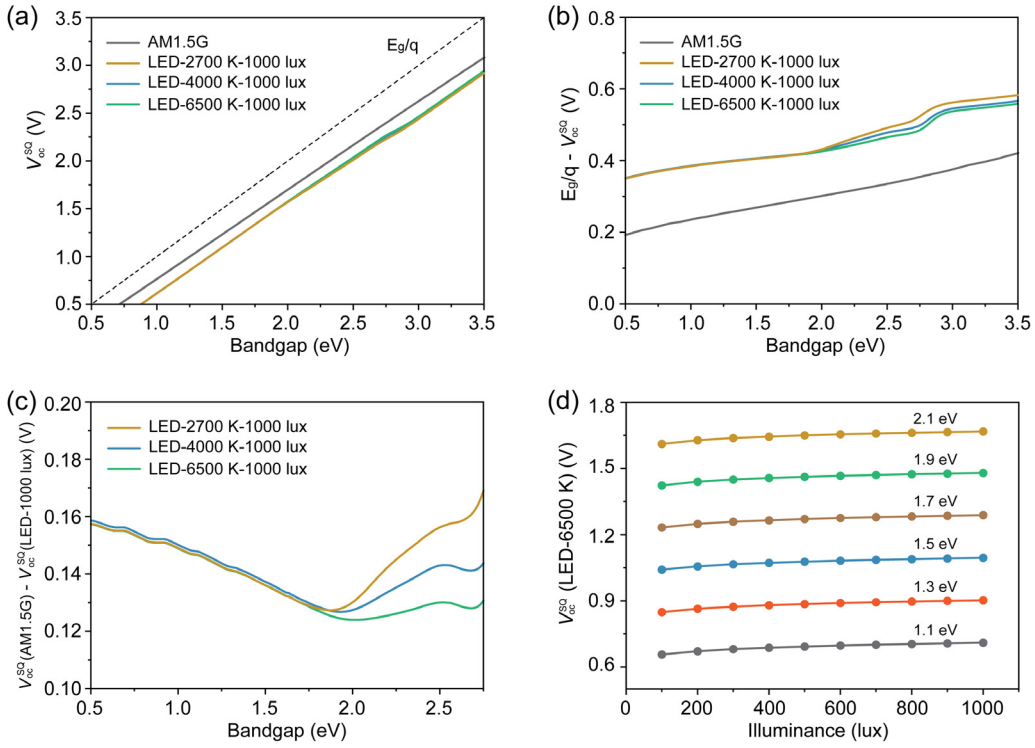

FIG. 3. Bandgap-dependent (a) SQ-limited V_{oc}^{SQ} and (b) ΔV_1 for AM1.5G solar and 2700, 4000, and 6500 K LEDs at 1000 lux. (c) ΔV_{oc}^{extra} of 2700, 4000, and 6500 K LEDs at 1000 lux. (d) Variation of V_{oc}^{SQ} with illuminance of the absorber materials with various bandgaps under 6500 K LED illumination.

16 November 2025 15:40:56

Published under an exclusive license by AIP Publishing

$$V_{oc}^{rad} = \frac{kT}{q}\ln\left(\frac{J_{sc}^{rad}}{J_0^{rad}} + 1\right) = \frac{kT}{q}\ln\left[\frac{q\int_0^{\infty} EQE_{PV}(E)\Phi_{light}(E)dE}{q\int_0^{\infty} EQE_{PV}(E)\Phi_{BB}(E)dE} + 1\right]. \quad (17)$$

The third component (ΔV_3) represents the non-radiative loss, calculated by subtracting V_{oc}^{actual} from V_{oc}^{rad}. In practical, ΔV_3 can be expressed as follows:[21]

$$\Delta V_3 = -\frac{kT}{q}\ln(EQE_{EL}), \quad (18)$$

where EQE_{EL} is the electroluminescence quantum efficiency of the PV cell. The schematic of three components of V_{loss} is shown in Fig. S5.

In addition to the three recombination-induced V_{oc} loss discussed earlier, there is an extra V_{oc} loss (ΔV_{oc}^{extra}) arising from the reduction in J_{sc} when transitioning from solar to indoor applications. This can be expressed as follows:

$$\Delta V_{oc}^{extra} = V_{oc}^{SQ}(AM1.5G) - V_{oc}^{SQ}(indoor) = \frac{kT}{q}\ln\left[\frac{J_{sc}^{SQ}(AM1.5G)}{J_{sc}^{SQ}(indoor)}\right]. \quad (19)$$

Figure 3(c) shows that ΔV_{oc}^{extra} between AM1.5G and LED conditions typically ranges from 0.13 to 0.18 V. ΔV_{oc}^{extra} is minimized at the bandgap of 1.8 eV, which corresponds to the bandgap where J_{sc}^{SQ} is exactly saturated under LEDs. Figure 3(d) indicates that V_{oc}^{SQ} varies slightly with illuminance when the bandgap is fixed.

We then shifted our focus to discussing FF. According to Eq. (7), the key to the expression of FF is the output power density of the PV cell ($P = JV$), where J can be expressed as follows:[25]

$$J(V) = J_0\left[\exp\left(\frac{qV}{nkT}\right) - 1\right] - J_{sc}. \quad (20)$$

Through Eq. (12), J_0 can be expressed as

$$J_0 = \frac{J_{sc}}{\exp\left(\frac{qV_{oc}}{kT}\right) - 1}. \quad (21)$$

By substituting Eq. (21) into Eq. (20), the $J(V)$ characteristic equation can also be described as follows:

$$J(V) = J_{sc}\left[1 - \frac{\exp\left(\frac{qV}{kT}\right) - 1}{\exp\left(\frac{qV_{oc}}{kT}\right) - 1}\right]. \quad (22)$$

We thereby obtained the expression of $P(V)$ as follows:

$$P(V) = VJ_{sc}\left[1 - \frac{\exp\left(\frac{qV}{kT}\right) - 1}{\exp\left(\frac{qV_{oc}}{kT}\right) - 1}\right]. \quad (23)$$

At the maximum power point, $\frac{dP(V)}{dV}$ is 0, from which we derive

$$V_m + \frac{kT}{q}\ln\left[\frac{qV_m}{kT} + 1\right] = V_{oc}, \quad (24)$$

where V_m is the voltage at the maximum power point. Now, we can rewrite Eq. (7) by combining Eqs. (23) and (24) and obtain the precise implicit relationship for FF,

$$FF = \frac{v_m}{v_m + 1}\cdot\frac{v_{oc} - \ln(v_m + 1)}{v_{oc}[1 - \exp(-v_{oc})]}, \quad (25)$$

where $v_m = \frac{V_m}{kT/q}$ and $v_{oc} = \frac{V_{oc}}{kT/q}$. In practice, v_{oc} is typically higher than 20, so that $\exp(-v_{oc})$ can be approximated as 0, and we can approximate $V_m = V_{oc}$ in Eq. (22),

$$FF = \frac{v_{oc} - \ln(v_{oc} + 1)}{v_{oc} + 1}. \quad (26)$$

Green demonstrated substituting "1" with "0.72" significantly enhances accuracy.[33] Additionally, the FF expression considering the effects of series (R_s) and shunt (R_{sh}) resistances is presented as follows:[33]

$$FF_0 = \frac{v_{oc} - \ln(v_{oc} + 0.72)}{v_{oc} + 1}\left(v_{oc} > 10,\ R_s = \frac{1}{R_{sh}} = 0\right), \quad (27)$$

$$FF_s = FF_0(1 - r_s) + \frac{r_s^2}{5.4}(v_{oc} > 10,\ r_s < 0.4,\ R_{sh} = \infty), \quad (28)$$

$$FF_{sh} = FF_0\left(1 - \frac{v_{oc} + 0.7}{v_{oc}}\frac{FF_0}{r_{sh}}\right)(v_{oc} > 10,\ r_{sh} > 2.5,\ R_s = 0), \quad (29)$$

$$FF_{s,sh} = FF_s\left(1 - \frac{v_{oc} + 0.7}{v_{oc}}\frac{FF_s}{r_{sh}}\right)\left(v_{oc} > 10,\ r_s + \frac{1}{r_{sh}} < 0.4\right), \quad (30)$$

where $r_s = \frac{R_s}{V_{oc}/J_{sc}}$, $r_{sh} = \frac{R_{sh}}{V_{oc}/J_{sc}}$. From the above-mentioned equations, FF is ideally a function of V_{oc} and hence bandgap dependent.

We then calculated SQ-limited FF (FF^{SQ}) under AM1.5 G illumination and 2700, 4000, and 6500 K LED conditions at 1000 lux by substituting V_{oc}^{SQ} in Eq. (27). Figure 4(a) shows that FF^{SQ} decreases as the bandgap decreases, maintaining $FF^{SQ} > 0.85$ for $E_g > 1$ eV. As E_g decreases below 1 eV, FF^{SQ} decreases rapidly. FF^{SQ} under AM1.5 G illumination is higher than that under LED illumination, primarily attributed to the higher V_{oc}^{SQ} under AM1.5G irradiation.

We further investigated the effects of R_s and R_{sh} on FF for bandgaps ranging from 1.1 to 2.1 eV. Figure 4(b) shows R_s-dependent FF_s under 6500 K LED illumination at 1000 lux, where $R_{sh} = \infty$. FF_s remains consistent when R_s is below 100 Ω cm^2. In contrast, under AM1.5G illumination, R_s should be reduced to below 1 Ω cm^2 to maintain consistent FF_s [Fig. S6(a)], representing a 100-fold decrease compared to the value under LED illumination. Figure 4(c) presents the R_{sh}-dependent FF_{sh} under the same LED illumination, where $R_s = 0$. FF_{sh} stabilizes when R_{sh} exceeds 100 kΩ cm^2. Conversely, under AM1.5G illumination, R_{sh} only needs to surpass 1.5 kΩ cm^2 to achieve stable FF_{sh} [Fig. S6(b)], corresponding to a 60-fold reduction relative to the requirements under LED illumination. These results demonstrate that: under indoor illumination, high FF requires larger R_{sh}, and FF remains insensitive to R_s up to 100 Ω cm^2; under solar illumination, high

16 November 2025 15:40:56

Published under an exclusive license by AIP Publishing

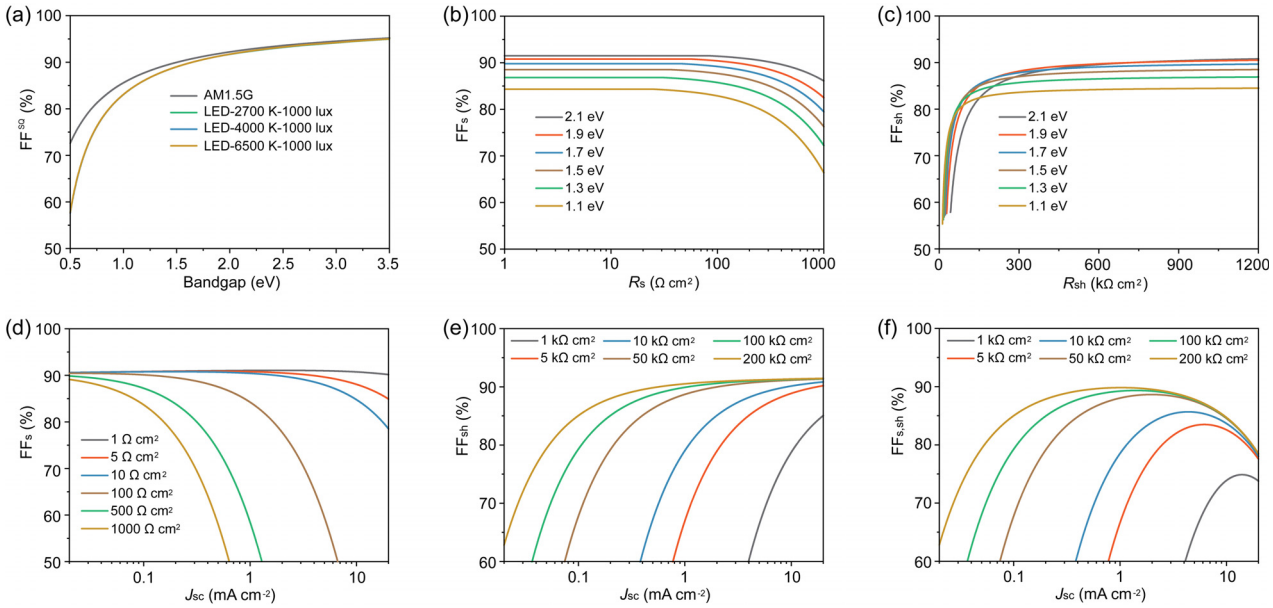

FIG. 4. (a) FF^{SQ} as a function of bandgap under AM1.5G and 2700, 4000, and 6500 K LEDs at 1000 lux. (b) Impact of R_s on FF ($R_{sh} = \infty$) and (c) impact of R_{sh} on FF ($R_s = 0$) under 6500 K LED at 1000 lux. (d) Variation of FF vs J_{sc} with various R_s ($R_{sh} = \infty$) and (e) various R_{sh} ($R_s = 0$). The optimized bandgap is 1.88 eV. (f) Variation of FF vs J_{sc} with various R_{sh} at $R_s = 10\ \Omega\ cm^2$.

FF necessitates lower R_s, while FF shows minimal dependence on R_{sh} above 1.5 kΩ cm^2. This divergence originates from the fact that under indoor illumination, J_{sc} is approximately one-thousandth of that under AM1.5G illumination. This leads to a proportional reduction in r_s and r_{sh} by a factor of 1000. Consequently, FF exhibits reduced sensitivity to R_s under indoor lighting conditions, while necessitating significantly larger values of R_{sh} to maintain optimal performance.

Based on the LED emission spectrum, we then selected a bandgap of 1.88 eV to investigate the influence of J_{sc} variations on FF_s and FF_{sh}. Figures 4(d) and 4(e) show that as J_{sc} decreases, FF_s increases while FF_{sh} decreases. We further investigated the combined effect of R_s and R_{sh} on FF. Figure 4(f) displays the J_{sc}-dependent $FF_{s,sh}$ under varying R_{sh} values at a fixed $R_s = 10\ \Omega\ cm^2$, with additional values of R_s shown in Fig. S7. The results reveal that as J_{sc} decreases (which in turn decreases linearly with the reduction in illuminance as discussed in Fig. 2), FF initially increases and then decrease, consistent with previous experimental results.[34]

After obtaining SQ-limited parameters of J_{sc}^{SQ}, V_{oc}^{SQ}, FF^{SQ}, and P_{in} of the incident light, we finally calculated SQ-limited PCE (PCE^{SQ}) of the photovoltaic cell using Eq. (5). Figure 5(a) shows the calculated PCE^{SQ} as a function of the absorber material's bandgap under AM1.5G illumination and LED illumination with CCTs of 2700, 4000, and 6500 K, at a fixed illuminance of 1000 lux. Under AM1.5G solar

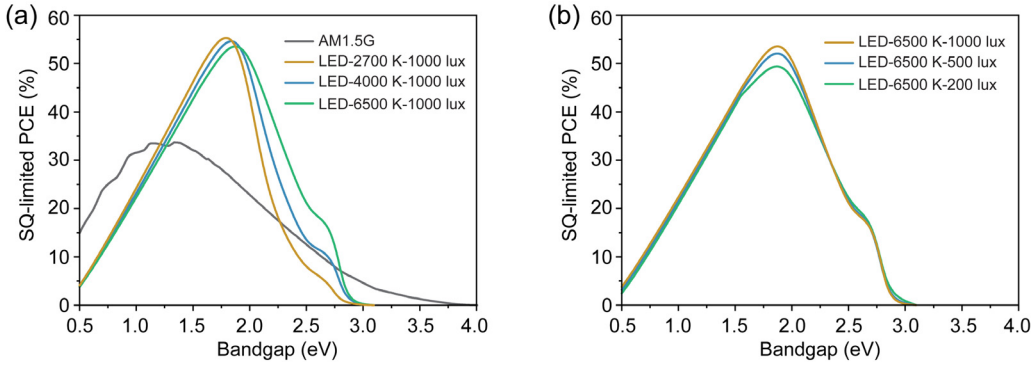

FIG. 5. (a) SQ-limited PCE as a function of bandgap under AM1.5G and 2700, 4000, and 6500 K LED at 1000 lux. (b) SQ-limited PCE as a function of bandgap under 6500 K LED at 200, 500, and 1000 lux.

16 November 2025 15:40:56

Published under an exclusive license by AIP Publishing

irradiance, the optimal bandgap for PV cells is 1.1–1.4 eV, achieving a PCE^{SQ} limit of ∼33%. In contrast, IPV devices under LED illumination (1000 lux) exhibit a significantly wider optimal bandgap of 1.8–1.9 eV, resulting in a higher PCE^{SQ} limit of approximately 55%, which is twice the PCE^{SQ} value under AM1.5G illumination (∼27%). Moreover, for the same light source, the optimal bandgap remains the same across different illuminance levels, with a slight decrease in PCE^{SQ} as illuminance decreases, arising from the linear reduction in J_{sc} and the consequent logarithmic decline in V_{oc} [Fig. 5(b)]. The higher PCE^{SQ} limit of IPV cells compared to that of solar cells arises from fundamental spectral differences: the narrow emission spectra of LEDs allow near-complete photon absorption with suppressed thermalization losses.

In summary, we systematically elucidate the fundamental device physics of IPVs through the SQ theory. By quantitatively comparing the spectra of standard solar irradiation (AM1.5G) and indoor light sources, we identify two critical distinctions: the significantly narrower spectral bandwidth (400–700 nm) and the three orders-of-magnitude lower light intensity characteristic of indoor illumination. Through further calculations of SQ-limited J_{sc}, V_{oc}, and FF, we reveal three cornerstone principles for IPV operation: (i) a linear scaling law between J_{sc} and illuminance, (ii) illuminance-independent V_{oc} behavior across practical illumination levels, and (iii) the necessity of ultrahigh R_{sh} to preserve a large FF. Based on these results, we finally determine the theoretical efficiency limits for IPVs, identifying an optimal bandgap range of 1.8–1.9 eV that enables a maximum PCE of ∼55% under LED illumination. This work not only establishes fundamental design principles for IPVs but also differentiates their operational device physics from conventional solar cells, thus providing critical guidance for high-performance IPVs.

See the supplementary material for further analysis details.

This work was supported by the National Key Research and Development Program of China (No. 2024YFB4205201), the National Natural Science Foundation of China (No. 22375206), and the Youth Innovation Promotion Association CAS (No. Y2021014).

AUTHOR DECLARATIONS

Conflict of Interest

The authors have no conflicts to disclose.

Author Contributions

Zhouqing Wei: Conceptualization (equal); Data curation (lead); Formal analysis (lead); Writing – original draft (lead). **Xin Wen:** Data curation (equal); Formal analysis (equal). **Wenbo Lu:** Data curation (equal); Formal analysis (equal); Writing – original draft (equal). **Xiaoyan An:** Data curation (equal); Formal analysis (equal). **Qingxiang Liu:** Data curation (equal); Formal analysis (equal). **Yunpei Zhang:** Data curation (equal); Formal analysis (equal). **Di Wu:** Data curation (equal); Formal analysis (equal). **Huan Yang:** Data curation (equal); Formal analysis (equal). **Jin-Song Hu:** Data curation (equal); Formal analysis (equal); Writing – review & editing (equal). **Ding-Jiang Xue:** Conceptualization (lead); Project administration (lead); Writing – review & editing (lead).

DATA AVAILABILITY

The data that support the findings of this study are available from the corresponding author upon reasonable request.

REFERENCES

[1]E. Hittinger and P. Jaramillo, "Internet of things: Energy boon or bane?," Science **364**, 326–328 (2019).
[2]S. Gong, Y. Lu, J. Yin, A. Levin, and W. Cheng, "Materials-driven soft wearable bioelectronics for connected healthcare," Chem. Rev. **124**, 455–553 (2024).
[3]H. Yu, N. Li, and N. Zhao, "How far are we from achieving self-powered flexible health monitoring systems: An energy perspective," Adv. Energy Mater. **11**, 2002646 (2021).
[4]J. Min, S. Demchyshyn, J. R. Sempionatto, Y. Song, B. Hailegnaw, C. Xu, Y. Yang, S. Solomon, C. Putz, L. E. Lehner, J. F. Schwarz, C. Schwarzinger, M. C. Scharber, E. Shirzaei Sani, M. Kaltenbrunner, and W. Gao, "An autonomous wearable biosensor powered by a perovskite solar cell," Nat. Electron. **6**, 630–641 (2023).
[5]Z. L. Wang, "Self-powered nanosensors and nanosystems," Adv. Mater. **24**, 280–285 (2012).
[6]R. Haight, W. Haensch, and D. Friedman, "Solar-powering the internet of things," Science **353**, 124–125 (2016).
[7]V. Pecunia, L. G. Occhipinti, and R. L. Z. Hoye, "Emerging indoor photovoltaic technologies for sustainable internet of things," Adv. Energy Mater. **11**, 2100698 (2021).
[8]I. Mathews, S. N. Kantareddy, T. Buonassisi, and I. M. Peters, "Technology and market perspective for indoor photovoltaic cells," Joule **3**, 1415–1426 (2019).
[9]C. Dong, X.-M. Li, C. Ma, W.-F. Yang, J.-J. Cao, F. Igbari, Z.-K. Wang, and L.-S. Liao, "Lycopene-based bionic membrane for stable perovskite photovoltaics," Adv. Funct. Mater. **31**, 2011242 (2021).
[10]K.-L. Wang, H. Lu, M. Li, C.-H. Chen, D. Bo Zhang, J. Chen, J.-J. Wu, Y.-H. Zhou, X.-Q. Wang, Z.-H. Su, Y.-R. Shi, Q.-S. Tian, Y.-X. Ni, X.-Y. Gao, S. M. Zakeeruddin, M. Grätzel, Z.-K. Wang, and L.-S. Liao, "Ion–dipole interaction enabling highly efficient $CsPbI_3$ perovskite indoor photovoltaics," Adv. Mater. **35**, e2210106 (2023).
[11]Q. Ma, Y. Wang, L. Liu, P. Yang, W. He, X. Zhang, J. Zheng, M. Ma, M. Wan, Y. Yang, C. Zhang, T. Mahmoudi, S. Wu, C. Liu, Y.-B. Hahn, and Y. Mai, "One-step dual-additive passivated wide-bandgap perovskites to realize 44.72%-efficient indoor photovoltaics," Energy Environ. Sci. **17**, 1637–1644 (2024).
[12]T. Zhang, C. An, Y. Xu, P. Bi, Z. Chen, J. Wang, N. Yang, Y. Yang, B. Xu, H. Yao, X. Hao, S. Zhang, and J. Hou, "A medium-bandgap nonfullerene acceptor enabling organic photovoltaic cells with 30% efficiency under indoor artificial light," Adv. Mater. **34**, 2207009 (2022).
[13]H. Li, Z. Zheng, S. Yang, T. Wang, Y. Yang, Y. Tang, S. Zhang, and J. Hou, "Anti-fatigue tandem organic photovoltaics for indoor illumination," Adv. Mater. **36**, 2311476 (2024).
[14]Y. Ren, D. Zhang, J. Suo, Y. Cao, F. T. Eickemeyer, N. Vlachopoulos, S. M. Zakeeruddin, A. Hagfeldt, and M. Grätzel, "Hydroxamic acid pre-adsorption raises the efficiency of cosensitized solar cells," Nature **613**, 60–65 (2023).
[15]P. R. Jebin, A. S. George, R. K. Mishra, J. John, and S. Soman, "Enhanced indoor photovoltaic efficiency of 40% in dye-sensitized solar cells using cocktail starburst triphenylamine dyes and dual-species copper electrolyte," J. Mater. Chem. A **12**, 32721–32734 (2024).
[16]B. Yan, X. Liu, W. Lu, M. Feng, H.-J. Yan, Z. Li, S. Liu, C. Wang, J.-S. Hu, and D.-J. Xue, "Indoor photovoltaics awaken the world's first solar cells," Sci. Adv. **8**, eadc9923 (2022).
[17]W. Lu, M. Feng, Z. Li, B. Yan, S. Wang, X. Wen, X. An, S. Liu, J.-S. Hu, and D.-J. Xue, "Ordering one-dimensional chains enables efficient selenium photovoltaics," Joule **8**, 1430–1442 (2024).
[18]W. Lu, Z. Li, M. Feng, J. Wei, X. Wen, X. An, Z. Wei, Y. Lin, J.-S. Hu, and D.-J. Xue, "Lanthanide-like contraction enables the fabrication of high-purity selenium films for efficient indoor photovoltaics," Angew. Chem., Int. Ed. **64**, e202413429 (2025).
[19]Q. Liu, X. Wang, Z. Li, W. Lu, X. Wen, X. An, M. Feng, H.-J. Yan, J.-S. Hu, and D.-J. Xue, "Standing 1D chains enable efficient wide-bandgap selenium solar cells," Adv. Mater. **37**, 2410835 (2025).

16 November 2025 15:40:56

Published under an exclusive license by AIP Publishing

[20]Y. Cui, L. Hong, T. Zhang, H. Meng, H. Yan, F. Gao, and J. Hou, "Accurate photovoltaic measurement of organic cells for indoor applications," Joule **5**, 1016–1023 (2021).
[21]Y. Cui, L. Hong, and J. Hou, "Organic photovoltaic cells for indoor applications: Opportunities and challenges," ACS Appl. Mater. Interfaces **12**, 38815–38828 (2020).
[22]A. Venkateswararao, J. K. W. Ho, S. K. So, S.-W. Liu, and K.-T. Wong, "Device characteristics and material developments of indoor photovoltaic devices," Mater. Sci. Eng., R **139**, 100517 (2020).
[23]P. R. Michael, D. E. Johnston, and W. A. Moreno, "Calculation of irradiance from illuminance for artificial light photovoltaics applications," IEEE Instrum. Meas. Mag. **26**, 52–58 (2023).
[24]J. K. W. Ho, H. Yin, and S. K. So, "From 33% to 57%—An elevated potential of efficiency limit for indoor photovoltaics," J. Mater. Chem. A **8**, 1717–1723 (2020).
[25]N. K. Elumalai and A. Uddin, "Open circuit voltage of organic solar cells: An in-depth review," Energy Environ. Sci. **9**, 391–410 (2016).
[26]W. Shockley and H. J. Queisser, "Detailed balance limit of efficiency of p-n junction solar cells," J. Appl. Phys. **32**, 510–519 (1961).
[27]J. Liu, S. Chen, D. Qian, B. Gautam, G. Yang, J. Zhao, J. Bergqvist, F. Zhang, W. Ma, H. Ade, O. Inganäs, K. Gundogdu, F. Gao, and H. Yan, "Fast charge separation in a non-fullerene organic solar cell with a small driving force," Nat. Energy **1**, 16089 (2016).
[28]A. Polman, M. Knight, E. C. Garnett, B. Ehrler, and W. C. Sinke, "Photovoltaic materials: Present efficiencies and future challenges," Science **352**, aad4424 (2016).
[29]S. Liu, J. Yuan, W. Deng, M. Luo, Y. Xie, Q. Liang, Y. Zou, Z. He, H. Wu, and Y. Cao, "High-efficiency organic solar cells with low non-radiative recombination loss and low energetic disorder," Nat. Photonics **14**, 300–305 (2020).
[30]M. A. Alam and M. R. Khan, *Principles of Solar Cells: Connecting Perspectives on Device, System, Reliability, and Data Science* (World Scientific, 2022).
[31]L. C. Hirst and N. J. Ekins-Daukes, "Fundamental losses in solar cells," Prog. Photovoltaics **19**, 286–293 (2011).
[32]M. A. Alam and M. R. Khan, "Fundamentals of PV efficiency interpreted by a two-level model," Am. J. Phys. **81**, 655–662 (2013).
[33]M. A. Green, "Accuracy of analytical expressions for solar cell fill factors," Sol. Cells **7**, 337–340 (1982).
[34]Y. Zhou, T. M. Khan, J. W. Shim, A. Dindar, C. Fuentes-Hernandez, and B. Kippelen, "All-plastic solar cells with a high photovoltaic dynamic range," J. Mater. Chem. A **2**, 3492–3497 (2014).

16 November 2025 15:40:56

Published under an exclusive license by AIP Publishing

Supplementary Material

Device physics of indoor photovoltaics: a fundamental investigation

Zhouqing Wei,[1,2] Xin Wen,[1,2] Wenbo Lu,[1,2] Xiaoyan An,[1,2] Qingxiang Liu,[1,2] Yunpei Zhang,[2] Di Wu,[2] Huan Yang,[3] Jin-Song Hu,[1,2] and Ding-Jiang Xue[1,2,a)]

[1]Beijing National Laboratory for Molecular Sciences (BNLMS), CAS Key Laboratory of Molecular Nanostructure and Nanotechnology, Institute of Chemistry, Chinese Academy of Sciences (CAS), Beijing 100190, China

[2]University of Chinese Academy of Sciences, Beijing 100049, China

[3]School of Chemistry and Materials Science, Shanxi Normal University, Taiyuan 030032, China

[a)]Authors to whom correspondence should be addressed: djxue@iccas.ac.cn

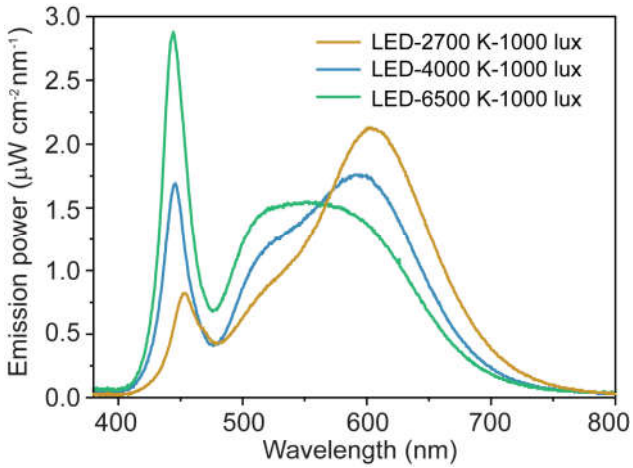

FIG. S1. Emission spectra of 2700 K, 4000 K and 6500 K LED at 1000 lux, respectively.

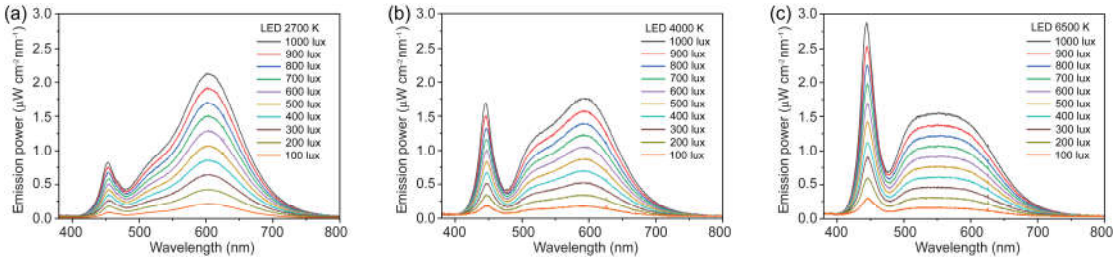

FIG. S2 Emission spectra of (a) 2700 K, (b) 4000 K and, (c) 6500 K LED under various illuminance.

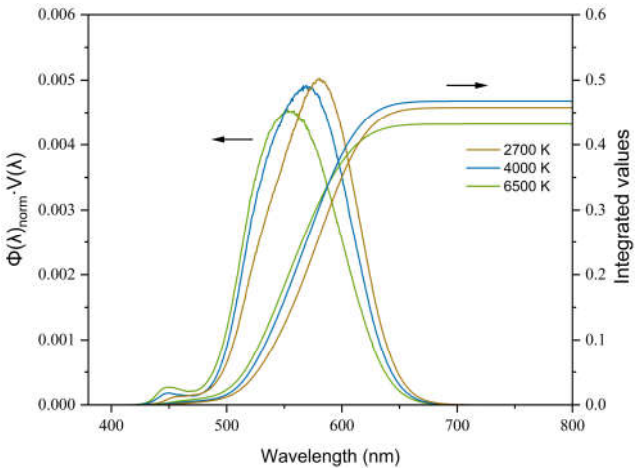

FIG. S3. $\Phi(\lambda)_{norm}V(\lambda)$ and integral values in equation (3) of 2700 K, 4000 K and 6500 K LEDs.

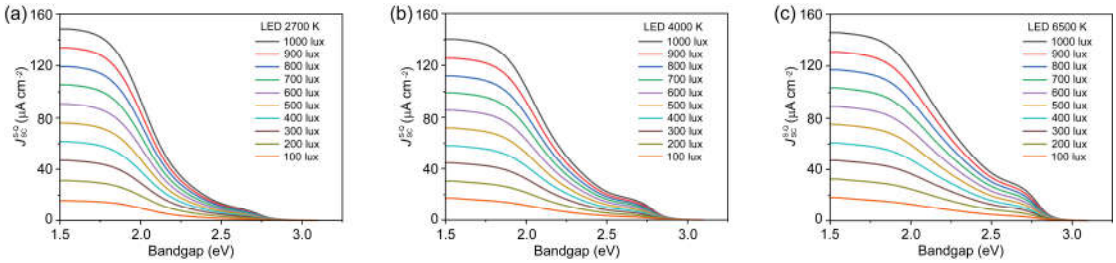

FIG. S4. Bandgap-dependent J_{sc}^{SQ} for (a) 2700 K, (b) 4000 K, and (c) 6500 K LED under various illuminance.

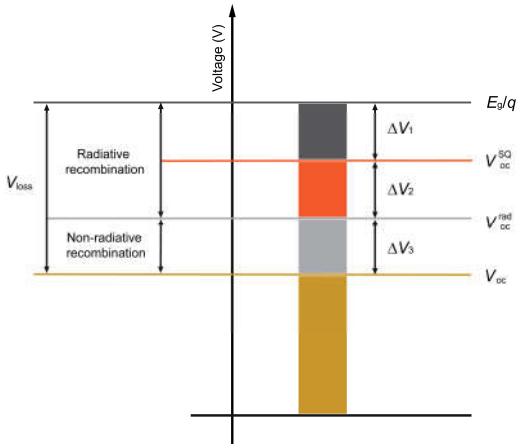

FIG. S5. Schematic of three components of V_{loss}.

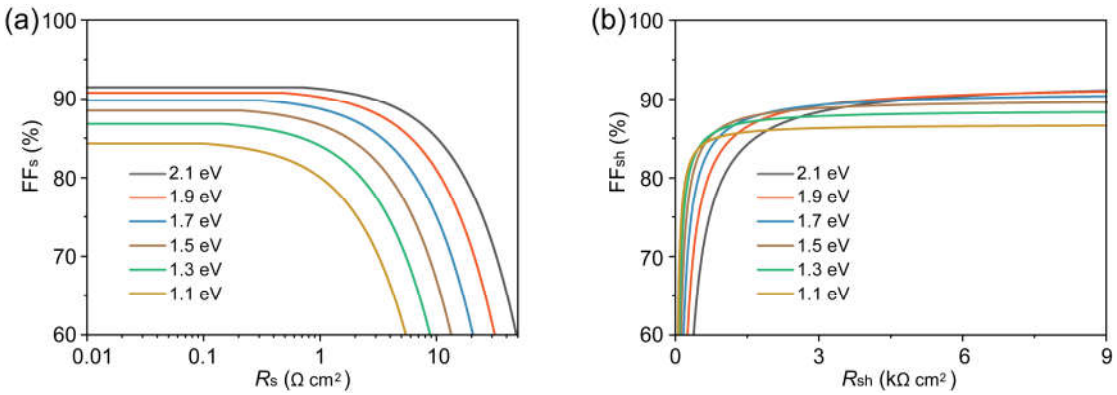

FIG. S6. (a) Impact of R_s on FF ($R_{sh} = \infty$) under AM1.5G. (b) Impact of R_{sh} on FF ($R_s = 0$) under AM1.5G.

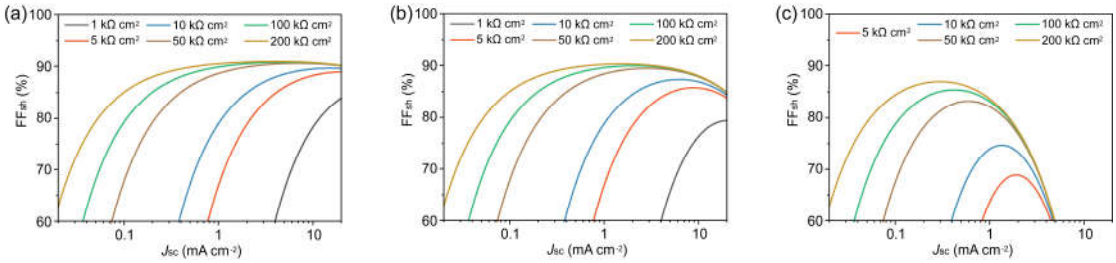

FIG. S7. The variation of FF versus J_{sc} with various R_{sh} for (a) R_s=1 Ω cm^2, (b) R_s= 5 Ω cm^2, and (c) R_s=100 Ω cm^2.